

## DISCLAIMER

This document was prepared as an account of work sponsored by the United States Government. While this document is believed to contain correct information, neither the United States Government nor any agency thereof, nor the Regents of the University of California, nor any of their employees, makes any warranty, express or implied, or assumes any legal responsibility for the accuracy, completeness, or usefulness of any information, apparatus, product, or process disclosed, or represents that

its use would not infringe privately owned rights. Reference herein to any specific commercial product, process, or service by its trade name, trademark, manufacturer, or otherwise, does not necessarily constitute or imply its endorsement, recommendation, or favoring by the United States Government or any agency thereof, or the Regents of the University of California. The views and opinions of authors expressed herein do not necessarily state or reflect those of the United States Government or any agency thereof or the Regents of the University of California.

# Numerical investigation of electron self-injection in the nonlinear bubble regime

C. Benedetti,<sup>1, a)</sup> C. B. Schroeder,<sup>1</sup> E. Esarey,<sup>1</sup> F. Rossi,<sup>2</sup> and W. P. Leemans<sup>1</sup>

<sup>1)</sup>*Lawrence Berkeley National Laboratory, Berkeley, California 94720, USA*

<sup>2)</sup>*University of Bologna and INFN, Via Irnerio 46, 40126 Bologna, Italy*

(Dated: 11 October 2013)

The process of electron self-injection in the nonlinear bubble wake generated by a short and intense laser pulse propagating in an uniform underdense plasma is studied by means of fully self-consistent particle-in-cell simulations and test-particle simulations. We consider a wake generated by a non-evolving laser driver traveling with a prescribed velocity, which then sets the structure and the velocity of the wake, so the injection dynamics is decoupled from driver evolution but a realistic structure for the wakefield is retained. We show that a threshold for self-injection into a non-evolving bubble wake exists, and we characterize the dependence of the self-injection threshold on laser intensity, wake velocity, and plasma temperature for a range of parameters of interest for current and future laser-plasma accelerators.

PACS numbers: 41.75.Jv, 52.35.Mw, 52.65.-y

## I. INTRODUCTION

Laser-plasma accelerators (LPAs) have received significant theoretical and experimental interest in the last several years<sup>1</sup> due to the possibility of producing low momentum spread (percent level) electron bunches with up to GeV energies in a short distance (a few millimeters/centimeters for  $\sim 0.1/1$  GeV electron energy)<sup>2-5</sup>. Their rapid development and properties make LPAs interesting candidates for applications to future high energy colliders<sup>6,7</sup> and radiation sources<sup>8-10</sup>. Most of the LPA experiments performed so far were carried out in the so called bubble regime<sup>11</sup>, in which the ponderomotive force of a short and intense laser pulse propagating in an underdense plasma transversally expels ambient electrons along its propagation path (ions can be considered at rest by virtue of their inertia) leading to the formation of a trailing ellipsoidal plasma cavity moving at relativistic velocity (bubble wake). Denoting by  $L_0$ ,  $I_0$ , and  $\lambda_0$  the r.m.s length, peak intensity, and wavelength of the laser pulse, respectively, the bubble regime can be accessed if  $k_p L_0 \sim 1$ , where  $k_p = \omega_p/c$ ,  $c$  is the speed of light in vacuum,  $\omega_p = (4\pi n_0 e^2/m)^{1/2}$  is the plasma frequency for a plasma of density  $n_0$  ( $m$  and  $e$  are, respectively, the electron mass and charge), and  $a_0 \gtrsim 2$ , where  $a_0 \simeq 8.5 \cdot 10^{-10} (I_0 [\text{W}/\text{cm}^2])^{1/2} \lambda_0 [\mu\text{m}]$  is the peak nor-

malized vector potential of the laser. The bubble, owing to its linearly varying longitudinal and transverse fields, has almost ideal accelerating and focusing properties for particles placed in the proper phase within the wake.

It has been observed in both experiments and 3D particle-in-cell (PIC) simulations, that in some cases electrons from the background plasma can be injected (self-injection) and accelerated in the bubble. Even though several techniques to promote/induce injection of background electrons have been developed (e.g., colliding pulses<sup>12,13</sup>, tailored density profiles<sup>14-16</sup>, ionization-induced injection<sup>17,18</sup>), self-injection is by far the simplest scheme from the experimental point of view. Understanding this process and the properties of the electron bunch at injection is of fundamental importance to control, and possibly improve or optimize, the performances of the LPA in view of future applications. Despite its relevance, a conclusive theory of particle self-injection and trapping in the 3D nonlinear bubble regime, which is drastically different from the nonlinear 1D regime<sup>19</sup>, is still missing even though several contributions have been proposed.<sup>20,21,23,26</sup> A numerical study presented in Ref. 20 first suggested that injection takes place for a sufficiently large bubble radius, namely  $R_{\text{bubble}} > 4$  (throughout the paper we use dimensionless units, normalizing the time to  $\omega_p^{-1}$ , the lengths to  $k_p^{-1}$ , the fields to  $m c \omega_p / e$ , the momenta to  $mc$ ). However, the dependence of the self-injection threshold on the wake phase velocity, which is suspected to play a ma-

<sup>a)</sup>cenedetti@lbl.gov

major role in the self-injection physics, was not discussed in this study. The self-injection process was analyzed in Ref. 21 through an analytic model which relates the injection condition to the bubble properties. In particular, assuming the simplified expression for the wakefield structure given in Ref. 22, and solving for the particle orbit in this field, it was found that self-injection occurs when  $\gamma_0 \lesssim R_{\text{bubble}}/\sqrt{2}$ , where  $\gamma_0$  is the Lorentz factor associated to a bubble wake moving with a (normalized) velocity  $\beta_0$ . In the case where the bubble is evolving,  $\gamma_0$  refers to value at the back of the bubble, where injection takes place. Assuming the relation given in Ref. 20 for the dependence of  $R_{\text{bubble}}$  from the laser driver in case of matched propagation, namely  $R_{\text{bubble}} \simeq w_0 \simeq 2\sqrt{a_0}$ , where  $w_0$  is the laser spot size, the injection threshold condition can be rewritten as  $a_0 \gtrsim \gamma_0^2/2$ . For  $\gamma_0 \sim 5-10$ , corresponding to a plasma density of  $n_0 \sim 10^{19}$  e/cm<sup>3</sup>, we have  $a_0 \gtrsim 10-50$ , which is rather high and not in accordance with both experiments and simulations. As mentioned in Ref. 21, this discrepancy is probably due to insufficient modeling of some key feature of the wakefield (e.g., field enhancement at the back of the bubble compared to the simple analytical linear expression).

A different analytical model for the self-injection is presented in Ref. 23. This model is also based on the simplified expression for the wakefield structure described in Ref. 22. However, the additional heuristic hypothesis is made that the orbits for the electrons reaching the back of the bubble (*i.e.* the ones that most likely will be injected) are elliptical. The injection threshold obtained in this case is  $R_{\text{bubble}} \gtrsim 2[\ln(2\gamma_0^2) - 1]^{1/2}$ , still showing a (weak) dependence on the wake phase velocity but with a significantly lower injection threshold for  $a_0$  compared to the result in Ref. 21 (in this case, for  $\gamma_0 \sim 5-10$ , the threshold for injection is  $a_0 \gtrsim 3.5-4$ ), and therefore it is in better agreement with experimental observations. A critical discussion of the two analytical models of Refs. 21 and 23, focusing in particular on the admissibility of the elliptical orbit hypothesis and its implications, can be found in Refs. 24 and 25.

While previous studies refer to a nonevolving bubble, all the discussed injection criteria can also be applied to the case of an evolving bubble, provided that the correct value for  $\gamma_0$ , the one at the back of the bubble, is used. In Ref. 26 Kalmykov *et al.* derived a sufficient condition for trapping in the case of an evolving bubble (*i.e.*, size and/or shape of the bubble are not constant) using a semianalytic nonstationary Hamiltonian theory. In particular, Kalmykov *et al.* showed analytically and by using PIC simulations that self-injection can be induced by a slow temporal expansion of the bubble. The existence of a minimum expansion rate which ensures trapping in a spherical bubble is also discussed.

The threshold for injection in the bubble regime has also been investigated in experiments<sup>27,28</sup>. In particular, in Ref. 27 it has been found that at low density ( $n_0 \simeq 3 \times 10^{18}$  cm<sup>-3</sup>) self-injection occurs when  $P/P_c > 4$ ,  $P$  and  $P_c$  being, respectively, the laser peak power and

the critical power for self-focusing ( $P_c[\text{GW}] \simeq 17\omega_0^2/\omega_p^2$ , where  $\omega_0 = 2\pi c/\lambda_0$ ). These experimental results are also supported by fully-self-consistent 3D PIC simulations. In Ref. 28 a detailed study of the dependence of the threshold for self-injection on laser-plasma parameters such as background plasma density, laser energy, pulse length, and focal spot quality is presented. However, an experimental approach, or even a set of fully-self-consistent PIC simulations of the experiment, does not provide, in general, enough insight on the self-injection mechanism owing to the complex interplay between injection physics, wake properties (phase velocity, amplitude) and laser evolution, and lacks generality.

In this paper, we present a systematic study of the self-injection process. We explore, by using fully-self-consistent PIC simulations under controlled conditions, the dependence of the injection physics from laser intensity, wake velocity, and background plasma temperature. In order to decouple injection physics from laser evolution we consider the bubble wake generated by a non-evolving Gaussian laser driver (with fixed shape and intensity) propagating in an uniform plasma with an assigned velocity. Provided that the laser-plasma interaction is turned on adiabatically (*i.e.*, the transient effects that manifest when the laser enters the plasma are suppressed), the wake generated by a non-evolving driver propagates at the driver's velocity and its shape and amplitude are constant. Under these controlled conditions we can determine when self-injection occurs and relate its appearance to the wake velocity and laser intensity (*i.e.*, wake size and amplitude). Our simulations show that an injection threshold exists for a cold plasma, even for a non-evolving bubble wake. In particular, for any given bubble phase velocity, we find that injection takes place if the laser intensity is high enough (*i.e.*, if the bubble size is large enough). We obtained empirically an expression for the intensity threshold value as a function of the wake velocity, namely  $a_0^*(\gamma_0)$ . The threshold is significantly lower than the one presented in Ref. 21, and it is in qualitative agreement with the one presented in Ref. 23 at low wake velocities ( $\gamma_0 \lesssim 60$ ). For  $\gamma_0$  large, we find that  $a_0^*$  grows linearly with  $\gamma_0$  so, as expected, self-injection does not occur in the ultra-relativistic limit ( $\gamma_0 \rightarrow \infty$ ).<sup>29</sup> Our results assume a non-evolving laser driver. If the driver evolves (due to diffraction, self-focusing, plasma wave guiding, self-steepening, depletion, *etc.*) the bubble wake velocity is no longer equal to the driver velocity but is determined by the driver evolution.<sup>30</sup> In this case, as previously discussed in Ref. 21, we show that the actual bubble phase velocity, which is dramatically different from the laser driver group velocity, is the relevant parameter to be considered for the self-injection physics. Finally, we investigate how the self-injection process is modified when the plasma has an initial non-zero temperature and we show that the self-injection threshold is reduced in a warm plasma.

All our simulations have been performed with the ponderomotive, 2D-cylindrical PIC code INF&RNO<sup>31-33</sup>.

Simulations with different numerical resolutions and different numbers of particle per cell have been considered in order to ensure reliable numerical results.

The paper is organized as follows. In Sec. II we describe the setup of our numerical calculations and we obtain the expression for the injection threshold in a non-evolving bubble wake for a cold plasma after presenting some general considerations on bubble geometry/shape. The properties of the transverse phase-space of the self-injected particles are also discussed. The phase velocity of the bubble wake generated by a self-consistently evolving laser pulse is discussed in Sec. III. A qualitative discussion on the influence of the background plasma temperature on the self-injection physics is discussed in Sec. IV. Conclusions are presented in Sec. V.

## II. SELF-INJECTION IN THE BUBBLE REGIME

### A. Simulation set up and numerical considerations

We consider a bubble wake generated by a non-evolving Gaussian laser-pulse propagating along the  $\hat{z}$  direction in an uniform underdense cold plasma with an assigned velocity  $\beta_0$ . The laser envelope is described by

$$a(z, r, t) = a_0 \exp\left(-\frac{r^2}{w_0^2}\right) \exp\left[-\frac{(z - z_0(t))^2}{4L_0^2}\right], \quad (1)$$

where  $z_0(t)$ , the laser centroid, evolves according to  $dz_0/dt = \beta_0$ . We fixed  $L_0 = 1$ , which is the linearly resonant length, and  $w_0 = 2\sqrt{a_0}$ , which is, as previously mentioned, the condition described in Ref. 20 for self-guided propagation of a short and intense laser pulse. If  $a_0 > 3$ , the nonlinear bubble wake generated behind the laser driver is approximately spherical with a size  $R_{\text{bubble}} \simeq w_0 = 2\sqrt{a_0}$ .<sup>20</sup> Since the laser pulse is non-evolving, the associated wake is stationary: the shape, size, and amplitude of the electromagnetic fields in the wake are constant and depend, nonlinearly, on  $a_0$ ,  $w_0$ , and  $L_0$ . The velocity of the wake is also constant and it is equal to the laser driver velocity  $\beta_0$ .<sup>30</sup> Using a non-evolving driver greatly simplifies the analysis of the injection physics. In contrast to a fully self-consistent simulation of the laser-plasma interaction process, laser evolution is decoupled from injection mechanism. In these controlled conditions, all the wake properties are specified once the laser driver properties are given. By tracking particle orbits, taking into account the ponderomotive force from the driver and the wakefields, we can determine under which conditions certain background plasma particles are self-injected and accelerated in the bubble.

From Refs. 21, 23–26, it is clear that the self-injection dynamics is very sensitive to fine-scale details of the field structure. However, accurate analytical expressions for the electromagnetic fields in the nonlinear bubble regime are not available<sup>29,34</sup>. To gain a better understanding of the injection process, we decided to evaluate numerically

the wakefield structure solving the Maxwell-Vlasov equations of the laser-plasma interaction by means of a PIC code. We used the 2D cylindrical, ponderomotive PIC code INF&RNO to evaluate the wakefield and compute the orbits of background plasma electrons. Cylindrical symmetry ( $r - z$ ) for both fields and particle orbits can be assumed in case of a round ponderomotive laser driver and a cold plasma. We performed a set of simulations for a range of laser-plasma parameters of interest for current and future LPA experiments. More specifically, we considered laser intensities corresponding to  $2 \leq a_0 \leq 7$ , and wake velocities corresponding to  $5 \leq \gamma_0 < 100$ .

In order to have well-controlled conditions and have a wake whose properties are unambiguously determined only by the velocity, the intensity, and the shape of the non-evolving driver, particular care has to be taken for the initialization of the simulation. If, for instance, we consider in our simulation a laser pulse that impinges from vacuum into a plasma slab, even if the driver is non-evolving, the associated wake shows, in the early stages of the laser-plasma interaction, time-dependent features. This stage, where the wake sets up and is not in equilibrium, typically requires a few tens of plasma periods. During this phase, depending on the details of the laser-plasma interaction, some of the background plasma electrons may remain trapped in the wake. Investigation of self-injection in these conditions is beyond the scope of this work. Indeed, in order for our numerical experiments to be successful and produce a bubble wake with well defined driver-dependent properties, self-injection in the early stages of the laser-plasma interaction needs to be inhibited. The presence of trapped particles located in the rear part of the bubble wake might affect the bubble properties through, for instance, beam loading, making difficult the interpretation of the results at later times when all the wake properties reach their stationary value. To prevent this effect, in our simulations we adiabatically turn on the laser-plasma interaction so the wake is smoothly formed. At the same time, we limit the maximum longitudinal velocity of the numerical particles to a value that is lower than the actual wake phase velocity, so self-injection in early stages is inhibited. While the laser-plasma interaction is turned on and the wake forms, the limit on the maximum particle velocity is gradually removed (typically this is done, for instance, by slowly ramping up the laser intensity and adding a sufficiently long density ramp at the entrance of the plasma). Injection of plasma particles is then fully enabled only after the wake properties have reached a stationary value. This procedure allows for a clean initialization of the bubble wake so all its properties depend only on the laser driver and any artifact related to simulation initialization is suppressed.

Studying the threshold for self-injection in case of a cold plasma using a PIC code can be numerically challenging due to the fact that simulation results can be affected by errors from statistical noise and finite space/time resolution. More specifically, as shown in

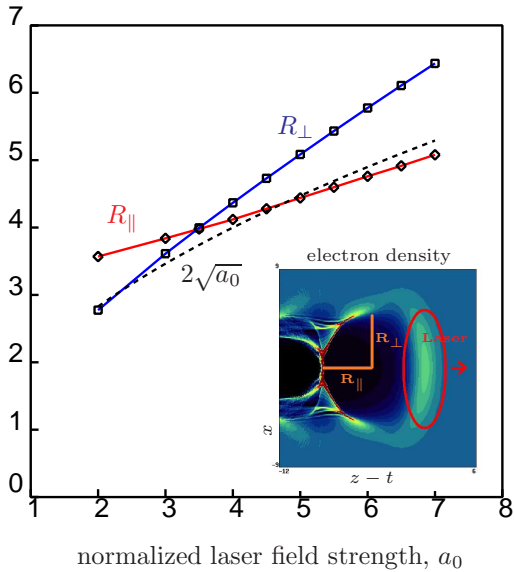


FIG. 1. Scaling of bubble radii (see inset for definition),  $R_{\perp}$  [squares] and  $R_{\parallel}$  [diamonds], with normalized laser field strength,  $a_0$ . The black dashed line is the quantity  $2\sqrt{a_0}$  which is the theoretical bubble size proposed in Ref. 20. The other laser-plasma parameters are  $L_0 = 1$ ,  $w_0 = 2\sqrt{a_0}$ , and  $\gamma_0 = 100$ . For  $\gamma_0 \gtrsim 10$ , the geometrical properties of the bubble are weakly dependence on  $\gamma_0$ , so the bubble shape can be simply characterized by  $a_0$ .

Ref. 35, PIC codes are prone to unphysical macroparticle trapping due to artificial heating. In order to quantify and keep under control these spurious numerical effects, we performed, for any given physical problem, different sets of simulations using different spatial resolutions and number of particles per cell. Denoting by  $\Delta z$  and  $\Delta r$ , respectively, the longitudinal and the transverse (radial) resolution, we considered the following set of numerical parameters in our simulations:  $\Delta z = \Delta r = 1/50$  with 25 particles/cell (low-resolution case),  $\Delta z = \Delta r = 1/100$  with 20 particles/cell (medium-resolution case), and, in selected cases,  $\Delta z = \Delta r = 1/200$  with 16 particles/cell (high-resolution case). From our simulations we observe that keeping a reasonably high transverse resolution, *i.e.*, at least  $\Delta r < 1/20$ , is very important to correctly capture the main features of self-injection dynamics. In the PIC code, force interpolation and current/charge deposition are performed with a quadratic scheme. We also use currents smoothing performed with a (1,2,1) binomial filter with compensator.

## B. Geometrical properties of the bubble wake

We have characterized the dependence of the bubble wake geometry from laser intensity. The wake shape/size can be characterized by the two radii,  $R_{\parallel}$  (longitudinal) and  $R_{\perp}$  (transverse), which are measured starting from

the center of the bubble (*i.e.*, the point where all the electromagnetic fields vanish). More specifically (see also the inset in Fig. 1),  $R_{\parallel}$  is the length of the accelerating part of the wake,  $R_{\perp}$  is the transverse width of the bubble defined as the transverse location where plasma density, almost zero on-axis, becomes equal to the background value. In Fig. 1 we show the functional dependence of  $R_{\parallel}$  and  $R_{\perp}$  from  $a_0$ , for  $2 \leq a_0 \leq 7$ . The other laser-plasma parameters were  $L_0 = 1$ ,  $w_0 = 2\sqrt{a_0}$ ,  $\gamma_0 = 100$ . We notice that, for  $\gamma_0 \gtrsim 10$ , the geometrical properties of the bubble are found to have a weak dependence on  $\gamma_0$  and so the bubble shape can be simply characterized by the peak laser field strength  $a_0$ . The black dashed line in Fig. 1 is the theoretical expression, given in Ref. 20,  $R_{\text{bubble}} \simeq R_{\parallel} \simeq R_{\perp} \simeq 2\sqrt{a_0}$ . It is worth noticing that the bubble shape is spherical only around  $a_0 \simeq 3.5$  (all the models presented in Refs. 21, 23, and 26 assume a spherical bubble), for  $a_0 \gtrsim 5$  significant deviations from the spherical shape are observed. Simulations show that  $R_{\parallel}$  depends linearly on  $a_0$ ; a numerical fit gives

$$R_{\parallel}(a_0) \simeq 2.9 + 0.305 \cdot a_0. \quad (2)$$

A linear dependence of  $R_{\parallel}$  on  $a_0$  can be inferred by using the 1D nonlinear theory, in spite of the fact that a 3D bubble wake has an inherently electromagnetic nature, while a 1D wake is purely electrostatic. In 1D, in the limit  $a_0 \gg 1$ , the longitudinal wakefield in any plasma wave period behind the laser driver is  $E_z(\zeta) \simeq \zeta/2$ , where  $\zeta$  is measured from the wake center, where the wakefield vanishes, and  $|\zeta| \leq \lambda_{Np}/2$ ,  $\lambda_{Np}$  being the nonlinear plasma wavelength.<sup>1</sup> The amplitude of the maximum accelerating field, measured at the back of the wake where  $\zeta = -\lambda_{Np}/2$ , is then  $E_{z,max} \simeq \lambda_{Np}/4$ , which can be rewritten as  $E_{z,max} \simeq R_{\parallel}/2$  after identifying  $\lambda_{Np}/2$  with  $R_{\parallel}$  (length of the accelerating part of the wake). On the other hand, if  $a_0 \gg 1$ , the maximum wakefield amplitude generated behind the laser driver is  $E_{z,max} \sim a_0$ , and so, qualitatively, we obtain the scaling  $R_{\parallel} \sim a_0$ .

## C. Location of the collection volume for self-injected particles

As noted in Refs. 36 and 37, self-injected electrons in the bubble wake are initially (*i.e.*, before the passage of the laser) located within a thin cylindrical shell volume (collection volume) with a radius that scales with the laser spot size and a width much smaller than the plasma skin-depth. These electrons, initially at rest, after receiving the ponderomotive kick from the laser driver, stream along the “wall” of the bubble wake reaching the back of the bubble where they are eventually injected and accelerated (see the inset in Fig. 2). In Fig. 2 we show (black diamonds) the location of the center of the collection volume,  $r_0$ , as a function of the peak normalized laser field strength,  $a_0$ , measured in simulations. Results refer to  $\gamma_0 = 10$ , however we found that  $r_0$  has a weak dependence on  $\gamma_0$  for  $\gamma_0 \gtrsim 10$ . The solid red line in Fig. 2 is a

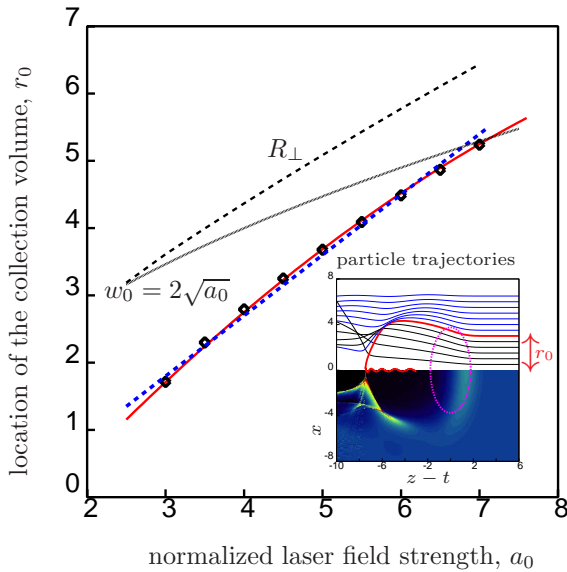


FIG. 2. Scaling of the location of the center of the collection volume for self-injected particles (see inset for definition),  $r_0$  [diamonds], with peak normalized laser field strength,  $a_0$ . The black dashed line is  $R_\perp$ , while the black solid line is the quasi-matched laser spot size, namely  $w_0 = 2\sqrt{a_0}$ . We can see that  $r_0$  scales with  $a_0$  as  $R_\perp$  rather than the laser spot size. The red solid line is the quadratic fit given by Eq. (3). The blue dashed line is the linear fit given by Eq. (4). The laser-plasma parameters are  $L_0 = 1$ ,  $\gamma_0 = 10$ . We found that  $r_0$  has a weak dependence on  $\gamma_0$  for  $\gamma_0 \gtrsim 10$ .

quadratic fit of the simulated data given by

$$r_0(a_0) \simeq -2.0 + 1.4 \cdot a_0 - 0.05 \cdot a_0^2. \quad (3)$$

A (more simple and less accurate) linear fit of the simulated points, given by

$$r_0(a_0) \simeq 0.9 \cdot (a_0 - 1), \quad (4)$$

is shown as a dashed blue line in Fig. 2. We notice that, qualitatively,  $r_0$  scales with  $a_0$  as the transverse bubble size ( $R_\perp$ , black dashed line in Fig. 2) rather than the laser spot size ( $w_0 = 2\sqrt{a_0}$ , black solid line). Equation (3) or Eq. (4) can be used as a guidance in PIC simulations of the bubble regime to selectively increase the numbers of numerical particle to be loaded in the region of the computational domain where the collection volume lies, and so to improve the statistical description of the self-injected beam.<sup>38,39</sup>

#### D. Threshold for self-injection

For the systematic study of the threshold for self-injection in the bubble regime, we performed several simulations corresponding to different points in the  $(\gamma_0, a_0)$  plane and, after carefully initializing each simulation with

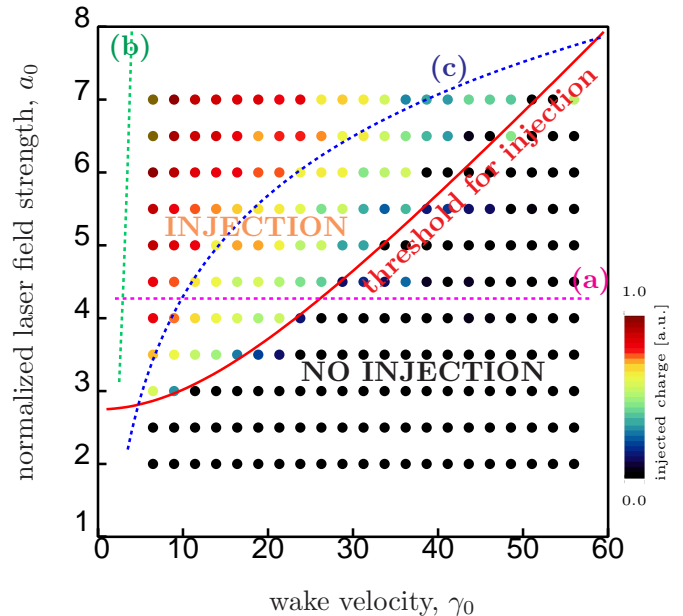


FIG. 3. Amount of self-injected charge in the bubble wake for different values of the wake velocity,  $\gamma_0$ , and normalized laser field strength,  $a_0$ . Each point is the outcome of a simulation run and the color is related to the amount of injected charge (black is no injection). The solid red line, which separates the injection and no-injection domains, is the empirical threshold condition for self-injection given by Eq. (5). The magenta dashed line (a) is threshold condition given in Ref. 20; the green dashed line (b) is the threshold condition given in Ref. 21; the blue dashed line (c) is the threshold condition given in Ref. 23.

the technique described in Sec. II A, we measured the amount of self-injected charge in the bubble wake for a fixed propagation length of the driver. Results are presented in Fig. 3. Each point is the outcome of a simulation and the color is related to the amount of injected charge (black is no injection). Two domains (injection vs. no-injection) are clearly identifiable and the boundary between them is marked by the solid red line. We find that, in case of a non-evolving laser driver, for any given bubble wake velocity, self-injection occurs provided that the peak laser field strength is above a threshold,  $a_0^*$ , which depends on the wake velocity. By combining results from all simulations, the expression for the injection threshold (solid red line in Fig. 3) is

$$a_0^*(\gamma_0) \simeq A_* \left[ 1 + (\gamma_0/\Gamma_*)^2 \right]^{1/2}, \quad (5)$$

where  $A_* = 2.75$  and  $\Gamma_* = 22$ . A clear dependence of the threshold from wake velocity is observed and, extrapolating in the limit where  $\gamma_0$  is large, we have  $a_0^*(\gamma_0) \sim (A_*/\Gamma_*)\gamma_0$ , so  $a_0^*(\gamma_0) \rightarrow \infty$  as  $\gamma_0 \rightarrow \infty$ . As expected, self-injection is not observed in the ultra-relativistic limit. The magenta dashed line (a) in Fig. 3 is the injection threshold from Ref. 20 (no  $\gamma_0$  dependence

is described). The green dashed line (b) is the threshold proposed in Ref. 21, namely  $a_0 \gtrsim \gamma_0^2/2$ , and qualitatively describes the same type of physics seen in our simulations (existence of a threshold for self-injection). However, our numerical results show a significantly lower value for the intensity threshold. For instance, for  $\gamma_0 = 20$ , the threshold for injection we obtain is  $a_0 \gtrsim 3.7$ , while the model presented in Ref. 21 predicts  $a_0 \gtrsim 200$ , which is rather high and not in agreement with experiments. This difference can be ascribed to the fact that the model in Ref. 21 adopts a simplified analytical expression for the bubble fields. In our model, a realistic field structure is retained, improving the description of electron's trajectories. More specifically, the model in Ref. 21 assumes the linear expression for the bubble fields given in Ref. 22, obtained for a traveling spherical cavity. However, the actual fields are only linearly varying in the center of the bubble and show a more complex (non-linearly varying) structure near the high-density plasma sheath surrounding the bubble wake (e.g., field enhancement at the back of the bubble in both longitudinal and transversal fields). The blue dashed line (c) in Fig. 3 is the threshold given in Ref. 23. Also this model assumes a spherical bubble wake and simplified linearly varying wakefields. The main difference from the model presented in Ref. 21 consists in the additional assumption, based on observations from PIC simulations, that the orbits of the particles reaching the back of the bubble are elliptical. The injection threshold obtained in Ref. 23 is significantly lower than the one in Ref. 21, and is in qualitative agreement with Eq. (5) when  $\gamma_0 \lesssim 60$ . However, our numerical results suggest a stronger dependence of the injection threshold on  $\gamma_0$ .

The threshold condition for self-injection given by Eq. (5) can also be rewritten in terms of a threshold condition for the laser power, namely  $P > P^*(\gamma_0)$ , where  $P^*(\gamma_0)$  is given by

$$\frac{P^*(\gamma_0)}{P_c} \simeq \frac{(w_0^* a_0^*)^2}{32} = \left(\frac{A_*}{2}\right)^3 \left[1 + (\gamma_0/\Gamma_*)^2\right]^{3/2}, \quad (6)$$

and where we assumed  $w_0^* = 2\sqrt{a_0^*}$ . We notice that, in case of a plasma with a background density  $n_0 \simeq 3 \times 10^{18}$  e/cm<sup>3</sup>, we can assume  $\gamma_0 \sim 10 - 20$  [as explained below, the exact value depends on the details of the (nonlinear) laser-plasma interaction] and so, using Eq. (6), the threshold for injection is  $P/P_c \gtrsim 4 - 6$ , which is in good agreement with the experimental value given in Ref. 27. At higher densities, i.e.,  $n_0 \gtrsim 10^{19}$  e/cm<sup>3</sup>, where we can assume  $\gamma_0 \ll \Gamma_*$ , we find that the threshold laser power for self-injection decreases to  $P/P_c \gtrsim 2.5$ , and this is also the overall absolute minimum power required for self-injection in the bubble regime.

### E. Test-particle simulations of self-injection

The self-injection threshold in the bubble regime can also be determined by means of test-particle simulations.

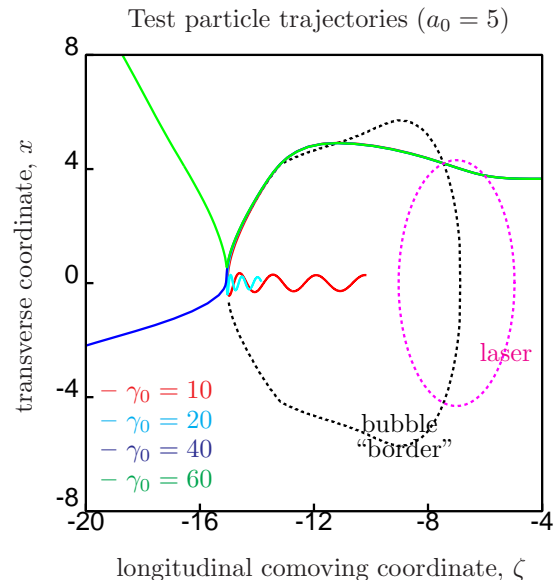


FIG. 4. Test-particle trajectories (same initial condition) for different values of the wake velocity, corresponding to  $\gamma_0 = 10$  (red), 20 (cyan), 40 (blue) and 60 (green), with  $a_0 = 5$ ,  $L_0 = 1$ , and  $w_0 = 2\sqrt{a_0}$ .

Here we integrate the equations of motion for a set of plasma particles (test-particles) under the effect of the ponderomotive force and the wakefields. In order to have a quantitatively correct description of self-injection, an accurate representation of the wakefield structure is required. Therefore, we use a numerical expression (wakefield map) computed from PIC simulations with frozen laser driver in the ultra-relativistic limit, where self-injection is absent and so the wake is unloaded. Using a wakefield map computed, for instance, when  $\gamma_0 = 1000$  to describe the wakefield at a lower wake velocity can be done since the wake structure has a weak dependence on the wake velocity, provided that the velocity remains relativistic (i.e.,  $\gamma_0 \gg 1$ ). A different wakefield map is required for any desired laser intensity. Assuming a test particle initially (i.e., before the passage of the laser) at rest in the  $(z, x)$  plane, and a round ponderomotive laser driver, then the trajectory of the test particle will remain in the same plane. The equations of motion for the test particles are

$$\begin{cases} \frac{d\zeta}{dt} = \frac{p_z}{\gamma} - \beta_0 \\ \frac{dx}{dt} = \frac{p_x}{\gamma} \\ \frac{dp_z}{dt} = -\frac{1}{2\gamma} \frac{\partial(a^2/2)}{\partial\zeta} + \frac{\partial\Psi}{\partial\zeta} - \frac{p_x}{\gamma} B_y \\ \frac{dp_x}{dt} = -\frac{1}{2\gamma} \frac{\partial(a^2/2)}{\partial x} + \frac{\partial\Psi}{\partial x} - \left(\beta_0 - \frac{p_z}{\gamma}\right) B_y \end{cases}, \quad (7)$$

where  $\zeta$  is the comoving longitudinal coordinate (using this coordinate the laser driver and the wakefield

are stationary),  $x$  is the transverse coordinate,  $p_z$  and  $p_x$  are, respectively, the longitudinal and transverse momentum of the test-particle,  $\gamma = (1 + a^2/2 + p_z^2 + p_x^2)$ ,  $\Psi$  is the wake potential, such that  $E_z = -\partial\Psi/\partial\zeta$  and  $E_x - \beta_0 B_y = -\partial\Psi/\partial x$ , where  $E_z, E_x, B_y$  are the components of the electromagnetic field in the wake. Both  $\Psi$  and  $B_y$  are taken from PIC simulations with  $\gamma_0 \gg 1$ . In particular,  $\Psi$  is computed from  $E_z$  at any transverse location  $x$ , according to  $\Psi(\zeta, x) = -\int_{+\infty}^{\zeta} E_z(\zeta', x) d\zeta'$ , where we assumed  $\Psi = 0$  ahead of the laser pulse. Using test particles simulations it is possible to explore, for any given  $a_0$  and  $\gamma_0$ , if and when self-injection appears. As an example, in Fig. 4 we show, for  $a_0 = 5$ , how the trajectory of a given test particle changes while changing the wake velocity (we considered  $\gamma_0 = 10, 20, 40, 60$ , see figure for details). Particle trajectories are qualitatively different for different  $\gamma_0$  and, as expected, no injection is observed at high  $\gamma_0$ . The self-injection threshold obtained exploring the  $(\gamma_0, a_0)$  parameter space with this technique is in good agreement with the expression given by Eq. (5).

### F. Hamiltonian analysis of the self-injection physics

The Hamiltonian describing the motion of a generic test particle in a given 3D wake is

$$H = \gamma - \beta_0 p_z - \Psi. \quad (8)$$

In case of a non-evolving wake  $H$  is a constant of motion. In particular,  $H = 1$  for a generic background plasma electron initially at rest. A particle is trapped if its longitudinal velocity equals the wake phase velocity while the particle is located within an accelerating and focusing domain of the wakefield. Denoting by  $\tilde{\zeta}, \tilde{x}, \tilde{p}_z, \tilde{p}_x, \tilde{\gamma}, \tilde{\Psi}$ , respectively, the longitudinal/transverse coordinate, the longitudinal/transverse momentum, the relativistic factor and the wake potential of a particle at moment of trapping, then, by definition,  $\tilde{u}_z/\tilde{\gamma} = \beta_0$ , and Eq. (8) with  $H = 1$  gives

$$\tilde{\Psi} \equiv \Psi(\tilde{\zeta}, \tilde{x}) = -1 + \frac{\sqrt{1 + (\tilde{p}_x)^2}}{\tilde{\gamma}}, \quad (9)$$

which expresses a necessary condition for trapping. In deriving Eq. (9) we assumed that self-injection takes place far behind the laser pulse where the laser field amplitude is negligible ( $a \simeq 0$ ). From Eq. (9) we see that trapping is facilitated, *i.e.* it requires a less negative potential to happen, at low phase velocities or when the particle has a large transverse momentum.

In Fig. 5 (a) we show, for  $a_0 = 5$ , the transverse phase space at the moment of injection,  $(\tilde{x}, \tilde{p}_x)$ , for a set of test particle simulations corresponding to different values of the wake velocity such that  $\gamma_0 = 10$  (black), 20 (red), 30 (blue). In Fig. 5 (b) we show, for a fixed wake velocity ( $\gamma_0 = 12$ ), the transverse phase space at injection for different values of the peak laser field strength, namely  $a_0 =$

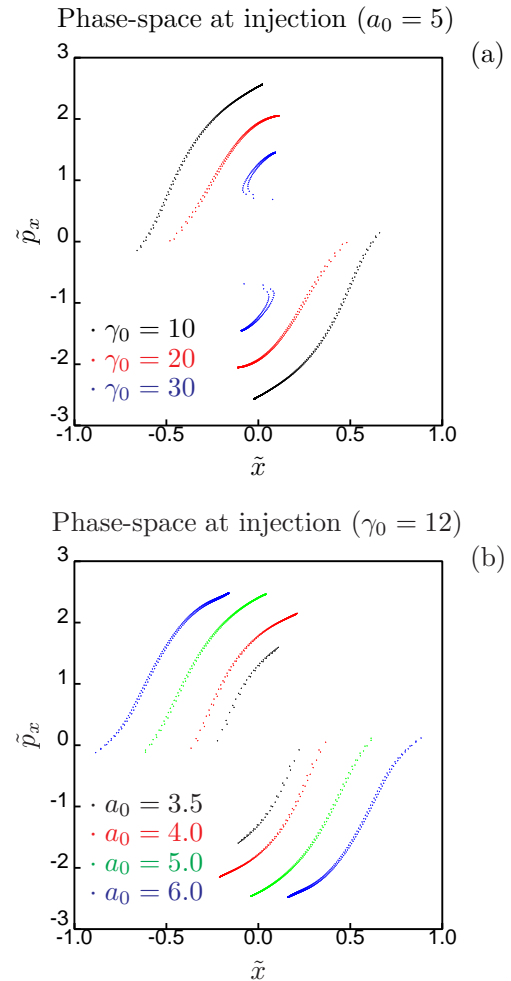


FIG. 5. Transverse phase space at moment of injection,  $(\tilde{x}, \tilde{p}_x)$ , for test-particle simulations with (a) fixed laser intensity ( $a_0 = 5$ ) and  $\gamma_0 = 10$  (black), 20 (red), 30 (blue). Simulations with (b) fixed wake velocity ( $\gamma_0 = 12$ ) and  $a_0 = 3.5$  (black), 4.0 (red), 5.0 (green), 6.0 (blue). The other laser-plasma parameters are  $L_0 = 1$ ,  $w_0 = 2\sqrt{a_0}$ .

3.5 (black), 4.0 (red), 5.0 (green), 6.0 (blue). Test particles were initially at rest (cold plasma) and uniformly distributed in a rectangular domain in the  $(z, x)$  plane located ahead of the laser pulse and encompassing the collection volume for self-injected particles for any value of  $a_0$ . The total number of particles used in each run depended on the size of the domain, typically we loaded 25 ( $= 5 \times 5$ ) - 100 ( $= 10 \times 10$ ) test particles within each cell of the grid over which the wakefields are defined. The lower (upper) lobe in the figures refers to particles initially laying in the  $x > 0$  ( $x < 0$ ) half-plane. We verified that Eq. (9) is satisfied for all trapped particles. We notice that particles at injection tend to have a rather high (relativistic) transverse momentum ( $|\tilde{p}_x| \sim 1 - 2$  for the parameters considered in this paper). Also, for fixed  $a_0$  and  $\gamma_0$ , the values of  $\tilde{x}$  and  $\tilde{p}_x$  are inversely correlated, so  $\tilde{p}_x$  tends to be larger (lower) if injections happens on-

axis (off-axis). Finally, the extent in phase space of the injection area becomes larger, for fixed  $a_0$ , the lower is the wake phase velocity or, for fixed  $\gamma_0$ , the higher is the laser intensity. This has implications in setting the value of the initial (*i.e.*, at injection) emittance for LPA beams in the bubble regime which we expect to be increasingly higher for laser-plasma parameters progressively away from the injection threshold given by Eq. (5).

### III. WAKE PHASE VELOCITY IN THE NONLINEAR REGIME

So far, in our study, the velocity of the bubble wake is assigned and determined solely by the velocity of the non-evolving ponderomotive laser driver. However, in case of a fully-self-consistent driver, the velocity of the wake generated by a short and intense laser pulse propagating in a plasma is different from the laser group velocity and is determined mainly by the laser driver evolution as well as by the background density.<sup>30</sup> In Fig. 6 (a) we show the evolution of the laser group velocity  $\gamma_{\text{laser}}(z)$  [red solid line] and wake phase velocity  $\gamma_0(z)$  measured at the center [blue solid line] and at the back [blue dashed line] of the bubble wake for a laser pulse with  $a_0 = 4.5$ ,  $L_0 = 1$ ,  $w_0 = 2\sqrt{a_0} = 4.2$ , and  $\omega_0/\omega_p = 90$ . The laser pulse is focused at the beginning of the plasma. The plasma profile is uniform after an initial linear ramp ( $L_{\text{ramp}} = 5$ ). The phase velocity at the center of the bubble has been measured by tracking the position of the on-axis point in the wake where the longitudinal field vanishes, and then computing numerically the  $z$ -derivative. The phase velocity at the back of the bubble is more difficult to measure owing to the fact that in this region the electromagnetic fields are rapidly varying in space (non-linear field structure). To obtain the estimate of the wake velocity shown in Fig. 6 (a) (blue dashed line), we first tracked, as before, the phase location of the point in the back of the wake where the longitudinal field is zero. Then we fitted the data with a high-order polynomial expression in  $z$ , and finally we computed the phase velocity taking the  $z$ -derivative of the fit. In Fig. 6(b) we plot the evolution of the peak normalized laser field strength  $a_0(z)$  over the same propagation length. The black dashed line in Fig. 6(a) is the linear theory prediction ( $a_0 \ll 1$ ) for the wake phase velocity, for which  $\gamma_0^{(\text{linear})} = \gamma_{\text{laser}}^{(\text{linear})} = \omega_0/\omega_p = 90$ . Analytical results describing, in 1D, laser and wake propagation when  $a_0 \gtrsim 1$  including the effects of pulse-steepening and frequency redshifting (*i.e.*, longitudinal pulse evolution) are discussed in Ref. 30. More specifically, it is found that in the early stages of the laser-plasma interaction, if  $a_0 \gg 1$ , the phase velocity of the back of the wake is  $\gamma_0^{(1D)} \simeq 0.45 \omega_0/\omega_p \simeq 40.5$  (magenta dashed line [i] in Fig. 6(a)). However, we expect the actual velocity of the wake to be lower than the 1D result, owing to the fact that there is transverse evolution of the laser drive due to self-focusing and the fact that differ-

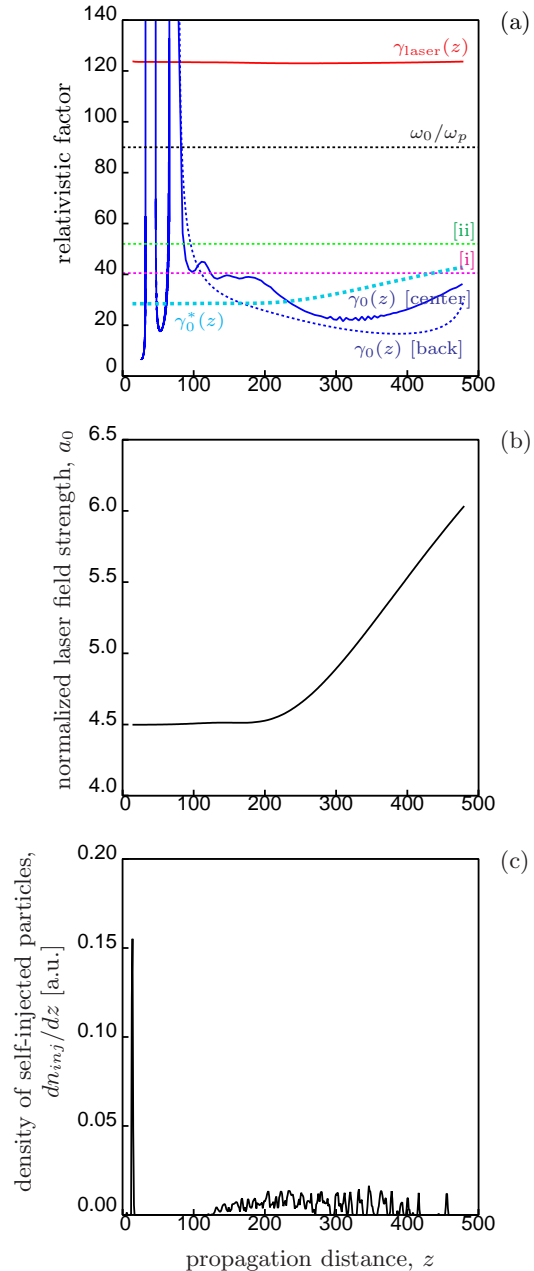


FIG. 6. Evolution (a) of the laser group velocity  $\gamma_{\text{laser}}(z)$  (red solid line), wake phase velocity  $\gamma_0(z)$  measured at the center (blue solid line) and at the back of the bubble (blue dashed line), and (b) normalized laser field strength  $a_0(z)$  (black solid line) for a fully-self-consistent simulation with  $a_0 = 4.5$ ,  $L_0 = 1$ ,  $w_0 = 2\sqrt{a_0} = 4.2$ , and  $\omega_0/\omega_p = 90$ . The black dashed line is the linear theory prediction for the wake velocity  $\gamma_0^{(\text{linear})} = \omega_0/\omega_p = 90$ , the magenta dashed line [i] is the 1D nonlinear wake velocity  $\gamma_0^{(1D)} \simeq 40.5$  given in Ref. 30, and the green dashed line [ii] is the value of  $\gamma_0^{(3D)} \simeq 52$  proposed in Ref. 20. The cyan dashed line is the  $z$ -dependent maximum wake velocity compatible with injection,  $\gamma_0^*(z)$ , computed via Eq. (5) using the normalized laser field strength  $a_0(z)$ . Distribution (c) of self-injected electrons as a function of their initial longitudinal position.

ent longitudinal slices of the driver experience a different degree of plasma wave guiding. This results in a modification of the laser intensity profile and hence of the shape of the wake. In 3D, an analytical theory of the nonlinear wake phase velocity is lacking. In Ref. 20, by using PIC simulations, Lu *et al.* propose, for the wake velocity generated by a quasi-matched laser pulse in the bubble regime, the constant value  $\gamma_0^{(3D)} \simeq \omega_0/\sqrt{3}\omega_p \simeq 52$  (green dashed line [ii] in Fig. 6(a)). From the simulation we observe that, initially, during bubble formation ( $z \lesssim 100$ ), the wake phase velocity exhibits large fluctuations. When the wake is formed and, as in this case, the laser pulse is intense ( $a_0 \gtrsim 1$ ), its velocity is determined mainly by the laser evolution resulting from the competition between laser self-focusing/diffraction, plasma wave guiding, self-steepening and frequency red-shifting. In our simulation conditions (laser at focus at the entrance of the plasma slab, with laser-plasma parameters typical of current LPAs), the bubble velocity is, as expected, lower than that of the driver and lower than the linear theory prediction. More specifically, the wake velocity, measured at the center or at the back of the bubble, settles around  $\gamma_0 \sim 18 - 25$ , while, for the laser driver,  $\gamma_{\text{laser}} \simeq 123$ . We also notice that the 1D nonlinear prediction  $\gamma_0^{(1D)}$  overestimates the value of the wake velocity, due to strong laser self-focusing and slice-dependent plasma wave guiding.

If the wake velocity evolution is slow enough (*i.e.*, the velocity does not change too much over the time a plasma particle interacts with the bubble wake) we can, at any time, determine if self-injection will occur using Eq. (5) where the local values of wake velocity and laser intensity are considered. Using this criteria, we computed, starting from the values of the peak normalized laser field strength given in Fig. 6(b), the maximum wake velocity,  $\gamma_0^*(z)$ , compatible with self-injection. The result is shown in Fig. 6(a) [cyan dashed line]. We expect self-injection to be possible if the actual bubble phase velocity  $\gamma_0(z)$  measured at the back of the bubble, where injection takes place, is lower than the threshold value  $\gamma_0^*(z)$ . This happens, according to Fig. 6(a), for  $z \gtrsim 150$  until almost  $z \sim 500$ . In Fig. 6(c) we show the distribution of self-injected electrons as a function of their initial longitudinal coordinate. We see that self-injection mainly occurs, as predicted, when the phase velocity is low, *i.e.*, for  $z \gtrsim 130$  until  $z \sim 480$ . The presence of trapped electrons within the bubble wake (beam loading) affects the properties of the wake itself (*e.g.*, shape, phase velocity of the back of the bubble) owing to the transverse electric and magnetic fields associated with the accelerating bunch which modify the trajectories of the plasma electrons reaching the back of the bubble. This feedback, depending on the amount of self-injected charge, may prevent additional injection. As a consequence, the threshold condition Eq. (5) can only be applied to predict self-injection if there is a sufficiently small amount of self-injected charge so the wakefield structure is approximately that of an unloaded wake.

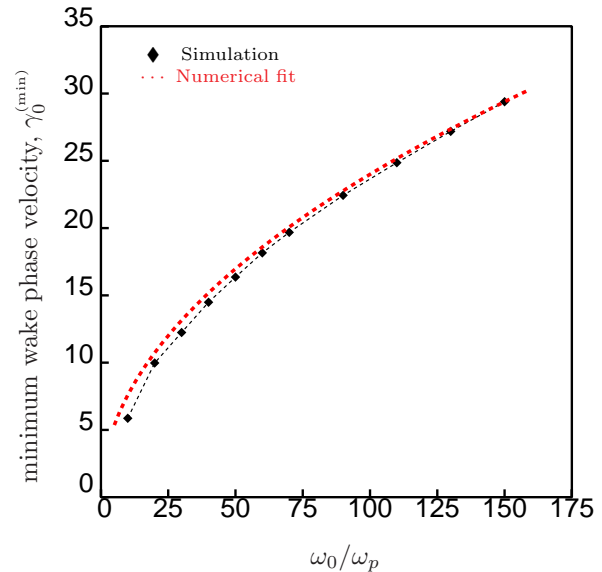


FIG. 7. Scaling of the minimum wake velocity measured at the center of the bubble wake,  $\gamma_0^{(min)}$  [diamonds], as a function of the background plasma density expressed in terms of  $\omega_0/\omega_p$ . The laser parameters at different densities satisfy  $L_0 = 1$  and  $w_0 = 2\sqrt{a_0}$ , with  $a_0 = 4.5$ . Even though the details of the phase velocity evolution depend on laser intensity, it is found in simulations that the minimum value of the phase velocity is independent from  $a_0$ . The red dashed line is the empirical fit of the minimum bubble velocity given by Eq. (10).

We investigated numerically the scaling of the minimum bubble phase velocity at the center of the wake,  $\gamma_0^{(min)}$ , changing the laser intensity and the background plasma density. We found that, if  $a_0 \gtrsim 2$ , the minimum value of the phase velocity is independent from  $a_0$ , even though the details of the phase velocity evolution depend on laser intensity. The scaling of  $\gamma_0^{(min)}$  with density is shown in Fig. 7, where we plot [black diamonds] the values of  $\gamma_0^{(min)}$  measured in a set of simulations with different plasma densities such that  $10 \lesssim \omega_0/\omega_p \lesssim 150$ . An empirical fit of the minimum bubble velocity is given by the simple formula [red dashed line in Fig. 7]

$$\gamma_0^{(min)} \simeq 2.4 \cdot \sqrt{\frac{\omega_0}{\omega_p}}. \quad (10)$$

Our study assumes a Gaussian laser driver but, as a consequence of transverse laser dynamics, the laser intensity profile evolves during propagation towards a “conical” shape (narrower towards the back).<sup>40</sup> The consequent change in the ponderomotive force affects particle orbits modifying the details of the self-injection process. Assessing the importance of this effect will be matter of future studies.

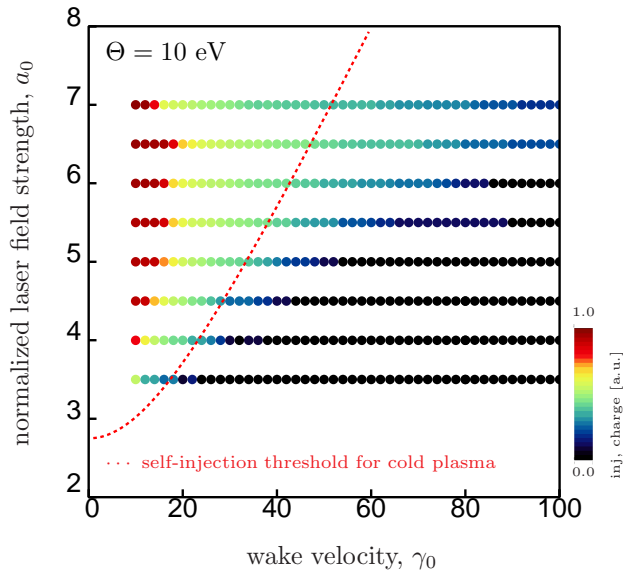


FIG. 8. Amount of self-injected charge in the bubble wake for different values of the wake velocity,  $\gamma_0$ , and normalized laser field strength,  $a_0$ , for a warm plasma ( $\Theta = 10$  eV). Each point is the outcome of a test-particle simulation run and the color is related to the amount of injected charge (black is no injection). The solid red line is the threshold condition for self-injection for a cold plasma given by Eq. (5). We notice that some degree of injection is present, for any given laser intensity, also for values of the phase velocity which are higher than the cold threshold value.

#### IV. SELF-INJECTION IN THE BUBBLE REGIME FOR A WARM PLASMA

Laboratory plasmas such the ones of interest for LPAs are not cold. For instance, the plasma created by a short and intense laser pulse ( $L_0 \sim 1$ ,  $a_0 \gtrsim 1$ ) through photoionization has a temperature of the order of the ionization potential, *i.e.*,  $\Theta \sim 10$  eV.<sup>41,42</sup> For LPAs, the laser-plasma interaction occurs on a time scale short compared to the ion motion and to the inverse of the collisional frequency. Such a collisionless plasma is not in local thermodynamical equilibrium. In this case plasma electrons experience relativistic motion (because of the intense laser field and wakefields) while the plasma temperature (momentum spread) remains small. In 1D, a relativistic warm plasma theory describing nonlinear laser-driven plasma waves has been presented in Ref. 43, and trapping of thermal plasma electrons is discussed in Ref. 19. Here we consider how the self-injection dynamics in a 3D bubble wake is modified in case of an initially warm plasma. We use a test-particle simulation approach, as described in Sec. II E, using the wakefield map computed for a cold plasma at different laser intensities, making the additional assumption that the wakefield structure will not be strongly affected by the background plasma temperature. The initial test-particle distribution is cho-

sen to be uniform in space (as described in Sec. II F) and Maxwellian in momentum. The total number of particles used in each run depended on the size of the domain, typically we loaded 100 - 400 test particles within each cell of the grid over which the wakefields are defined. Results are presented in Fig. 8, where each point is the outcome of a test-particle simulation in the  $(\gamma_0, a_0)$  parameter space, and the color is related to the amount of injected charge (black is no injection) for a warm plasma with  $\Theta = 10$  eV. The red dashed line is the threshold Eq. (5) obtained from fully-self consistent simulations of a cold plasma. We notice that some degree of injection is present for values of the phase velocity which are higher than the threshold value given by Eq. (5). The effect of the temperature becomes more important at higher laser intensities (*i.e.*,  $a_0 \gtrsim 5.5$ ).

#### V. CONCLUSIONS

In this paper we presented a detailed numerical investigation, by means of fully self-consistent PIC simulations and test-particle simulations, of electron self-injection in the bubble regime for a cold plasma. We studied the dependence of the injection threshold on peak laser field strength,  $a_0$ , and wake velocity,  $\beta_0 = (1 - 1/\gamma_0^2)^{1/2}$ , for a range of parameters of interest for current and future LPAs, namely  $2 \leq a_0 \leq 7$  and  $10 \leq \gamma_0 \leq 100$ . In particular, we considered the wake generated by a short ( $L_0 \sim 1$ ) and intense ( $a_0 > 1$ ) non-evolving Gaussian laser driver ( $w_0 = 2\sqrt{a_0}$ ) propagating with a constant velocity in an uniform plasma. Using a non-evolving driver has the twofold advantage that (1) self-injection physics is decoupled from driver evolution and (2) all the properties of the wake (*e.g.*, shape, size, amplitude of the electromagnetic fields, velocity) are determined univocally by the properties of the laser driver, provided that the laser-plasma interaction is turned on adiabatically in the simulation. Under these controlled conditions we determined that, for a non-evolving driver, self-injection occurs, and we explored the dependence of the threshold for self-injection on laser driver intensity and wake velocity. We obtained, numerically, that for any given value of the wake velocity the minimum laser intensity required for self-injection is  $a_0^* \simeq A_* [1 + (\gamma_0/\Gamma_*)^2]^{1/2}$ , where  $A_* \simeq 2.75$  and  $\Gamma_* \simeq 22$ . We found, as expected, that in the ultrarelativistic limit,  $\gamma_0 \rightarrow \infty$ , self-injection does not occur since  $a_0^* \rightarrow \infty$ . The threshold condition for self-injection can also be rewritten as a condition on the laser power. For instance, for a plasma with  $n_0 \simeq 3 \times 10^{18}$  e/cm<sup>3</sup>, we found that the minimum power required for self-injection is such that  $P/P_c \gtrsim 4-6$ . The calculation is in agreement with experimental results.<sup>27</sup> Together with the self-injection threshold we also analyzed the scaling of the bubble shape and size with the laser intensity, showing that significant differences from a round bubble wake are observed when  $a_0 \gtrsim 5$ . Finally, we characterized the dependence of the location of the center of the collection volume (*i.e.*, the

volume where the particles that will be self-injected are initially located) on the laser intensity. Results obtained in this case can be used to improve PIC simulations of the bubble regime by selectively increasing the number of numerical particles to be loaded in the region of the computational domain where the collection volume lies, and so to improve the statistical description of the self-injected beam.

The self-injection physics has been analyzed also by means of test-particle simulations, where the trajectory of a generic plasma particle is integrated taking into account the ponderomotive push from the driver and the stationary electromagnetic fields associated to the bubble wake. The description (map) of the wakefields is obtained, for any given  $a_0$ , from fully-self consistent PIC simulations in the ultrarelativistic limit, where injection is absent and so the bubble wake is unloaded. Since the structure of the wakefield is a weak function of  $\gamma_0$ , provided that  $\gamma_0 \gg 1$ , we used the same wakefield map to analyze the phase velocity dependence of test-particle trajectories. Even with this simplified approach (the wake velocity is the only free parameter once the laser intensity, and so the wakefield map, is fixed) we found that self-injection occurs at low wake velocity, in agreement with the threshold condition for self-injection described in Sec. IID. Test-particle simulations also allow to perform a Hamiltonian analysis of the trapping process. In particular, we verified that for trapped particles at moment of injection the condition  $\tilde{\Psi} = -1 + \sqrt{1 + (\tilde{p}_x)^2}/\gamma_0$  holds. Furthermore, we showed that particles at injection have a high (relativistic) transverse momentum and that the extent (spread) in phase space of the injection area becomes larger at low wake phase velocity and/or high laser intensity. This has implications in setting the initial (i.e., at injection) value of the emittance for LPA beams in the bubble regime which, consequently, we expect to be increasingly higher for laser-plasma parameters progressively beyond the self-injection threshold.

The threshold for self-injection has been derived in case of a non-evolving laser driver. If the driver evolves (because of self-focusing, plasma wave guiding and/or self-steepening), the bubble wake velocity is no longer equal to the driver velocity but is determined by its evolution. In this case, provided that the evolution rate is slow enough, we have shown that the actual bubble phase velocity, which is, in general, significantly different from the laser driver group velocity, is the relevant parameter to be considered for the self-injection physics. Even though the evolution of wake velocity shows a complex behavior due to the interplay of different nonlinear effects, we have shown that, in our conditions, the minimum wake velocity measured at the center of the wake in simulations can be expressed by the simple expression  $\gamma_0^{(\min)} \simeq 2.4(\omega_0/\omega_p)^{1/2}$ , and this value is independent of  $a_0$ .

Our study assumed a transverse Gaussian intensity profile for the laser driver. However, during propagation, the laser intensity profile evolves towards a “conical” shape (narrower towards the back). The resulting change in the ponderomotive force affects particle orbits and modifies the details of the self-injection process. Assessing the importance of this effect will be done in future studies.

Finally, we investigated how the self-injection dynamics in a 3D bubble wake is affected by a plasma with an initially non-zero temperature. We found that the self-injection threshold for a warm plasma is lower than the one for a cold plasma. The effect is relevant for the correct interpretation of PIC simulation results, since simulations at low resolution or with a low order interpolation scheme for force/current/charge evaluation always show some degree of numerical heating which may result in artificial/spurious self-injection and, consequently, in an incorrect description of LPAs physics.

## ACKNOWLEDGMENTS

We would like to thank C. G. R. Geddes, M. Chen, S. Rykovanov, B. H. Shaw and L. Yu for useful discussions and suggestions. This work was supported by the Director, Office of Science, Office of High Energy Physics, of the U.S. DOE under Contract No. DE-AC02-05CH11231, and used the computational facilities (Hopper, Edison) at the National Energy Research Scientific Computing Center (NERSC).

- <sup>1</sup>E. Esarey, C.B. Schroeder, and W.P. Leemans, *Rev. Mod. Phys.* **81**, 1229 (2009).
- <sup>2</sup>S. P. D. Mangles, C. D. Murphy, Z. Najmudin, A. G. R. Thomas, J. L. Collier, A. E. Dangor, E. J. Divall, P. S. Foster, J. G. Gallacher, C. J. Hooker, D. A. Jaroszynski, A. J. Langley, W. B. Mori, P. A. Norreys, F. S. Tsung, R. Viskup, B. R. Walton, and K. Krushelnick, *Nature* **431**, 535 (2004).
- <sup>3</sup>C. G. R. Geddes, Cs. Tóth, J. van Tilborg, E. Esarey, C. B. Schroeder, D. Bruhwiler, C. Nieter, J. Cary, and W. P. Leemans, *Nature* **431**, 538 (2004).
- <sup>4</sup>J. Faure, Y. Glinec, A. Pukhov, S. Kiselev, S. Gordienko, E. Lefebvre, J.-P. Rousseau, F. Burgy, and V. Malka, *Nature* **431**, 541 (2004).
- <sup>5</sup>W. P. Leemans, B. Nagler, A. J. Gonsalves, C. Tóth, K. Nakamura, C. G. R. Geddes, E. Esarey, C. B. Schroeder, and S. M. Hooker, *Nature Phys.* **2**, 696 (2006).
- <sup>6</sup>W. P. Leemans and E. Esarey, *Phys. Today* **62**, 44 (2009).
- <sup>7</sup>C. B. Schroeder, E. Esarey, C. G. R. Geddes, C. Benedetti, and W. P. Leemans, *Phys. Rev. ST Accel. Beams* **13**, 101301 (2010).
- <sup>8</sup>W. P. Leemans, C. G. R. Geddes, J. Faure, Cs. Tóth, J. van Tilborg, C. B. Schroeder, E. Esarey, G. Fubiani, D. Auerbach, B. Marcellis, M. A. Carnahan, R. A. Kaindl, J. Byrd, and M. C. Martin, *Phys. Rev. Lett.* **91**, 074802 (2003).
- <sup>9</sup>A. Rousse, K. T. Phuoc, R. Shah, A. Pukhov, E. Lefebvre, V. Malka, S. Kiselev, F. Burgy, J.-P. Rousseau, D. Umstadter, and D. Hulin, *Phys. Rev. Lett.* **93**, 135005 (2004).
- <sup>10</sup>M. Fuchs, R. Weingartner, A. Popp, Z. Major, S. Becker, J. Osterhoff, I. Cortrie, B. Zeitler, R. Hörlei, G. D. Tsakiris, U. Schramm, T. P. Rowlands-Rees, S. M. Hooker, D. Habs, F. Krausz, S. Karsch, and F. Grüner, *Nature Phys.* **5**, 826 (2009).
- <sup>11</sup>A. Pukhov and J. Meyer-ter-Vehn, *Appl. Phys. B* **74**, 355 (2002).
- <sup>12</sup>E. Esarey, R. F. Hubbard, W. P. Leemans, A. Ting, and P. Sprangle, *Phys. Rev. Lett.* **79**, 2682 (1997).
- <sup>13</sup>J. Faure, C. Rechatin, A. Norlin, A. Lifschitz, Y. Glinec, and V. Malka, *Nature* **444**, 737 (2006).

- <sup>14</sup>S. Bulanov, N. Naumova, F. Pegoraro, and J. Sakai, *Phys. Rev. E* **58**, R5257 (1998).
- <sup>15</sup>C. G. R. Geddes, K. Nakamura, G. R. Plateau, Cs. Tóth, E. Cormier-Michel, E. Esarey, C. B. Schroeder, J. R. Cary, and W. P. Leemans, *Phys. Rev. Lett.* **100**, 215004 (2008).
- <sup>16</sup>A. J. Gonsalves, K. Nakamura, C. Lin, D. Panassenko, S. Shiraishi, T. Sokollik, C. Benedetti, C. B. Schroeder, C. G. R. Geddes, J. van Tilborg, J. Osterhoff, E. Esarey, Cs. Tóth, and W. P. Leemans, *Nature Phys.* **7**, 862 (2011).
- <sup>17</sup>A. Pak, K. A. Marsh, S. F. Martins, W. Lu, W. B. Mori, and C. Joshi, *Phys. Rev. Lett.* **104**, 025003 (2010).
- <sup>18</sup>C. McGuffey, A. G. R. Thomas, W. Schumaker, T. Matsuoka, V. Chvykov, F. J. Dollar, G. Kalintchenko, V. Yanovsky, A. Maksimchuk, K. Krushelnick, V. Yu. Bychenkov, I. V. Glazyrin, and A. V. Karpeev, *Phys. Rev. Lett.* **104**, 025004 (2010).
- <sup>19</sup>C. B. Schroeder, E. Esarey, B. A. Shadwick, and W. P. Leemans, *Phys. Plasmas* **13**, 033103 (2006).
- <sup>20</sup>W. Lu, M. Tzoufras, C. Joshi, F. S. Tsung, W. B. Mori, J. Vieira, R. A. Fonseca, and L. O. Silva, *Phys. Rev. ST Accel. Beams* **10**, 061301 (2007).
- <sup>21</sup>I. Kostyukov, E. Nerush, A. Pukhov, and V. Seredov, *Phys. Rev. Lett.* **103**, 175003 (2009).
- <sup>22</sup>I. Kostyukov, A. Pukhov, and S. Kiselev, *Phys. Plasmas* **11**, 5256 (2004).
- <sup>23</sup>A. G. R. Thomas, *Phys. Plasmas* **17**, 056708 (2010).
- <sup>24</sup>S. Corde, A. Stordeur, and V. Malka, *Phys. Plasmas* **18**, 034701 (2011).
- <sup>25</sup>A. G. R. Thomas, *Phys. Plasmas* **18**, 034702 (2011).
- <sup>26</sup>S. Kalmykov, S. A. Yi, V. Khudik, and G. Shvets, *Phys. Rev. Lett.* **103**, 135004 (2009).
- <sup>27</sup>D. H. Froula, C. E. Clayton, T. Döppner, K. A. Marsh, C. P. J. Barty, L. Divol, R. A. Fonseca, S. H. Glenzer, C. Joshi, W. Lu, S. F. Martins, P. Michel, W. B. Mori, J. P. Palastro, B. B. Pollock, A. Pak, J. E. Ralph, J. S. Ross, C. W. Siders, L. O. Silva, and T. Wang, *Phys. Rev. Lett.* **103**, 215006 (2009).
- <sup>28</sup>S. P. D. Mangles, G. Genoud, M. S. Bloom, M. Burza, Z. Najmudin, A. Persson, K. Svensson, A. G. R. Thomas, and C.-G. Wahlström, *Phys. Rev. ST Accel. Beams* **15**, 011302 (2012).
- <sup>29</sup>S. A. Yi, V. Khudik, C. Siemon, and G. Shvets, *Phys. Plasmas* **20**, 013108 (2012).
- <sup>30</sup>C. B. Schroeder, C. Benedetti, E. Esarey, and W. P. Leemans, *Phys. Rev. Lett.* **106**, 135002 (2011).
- <sup>31</sup>C. Benedetti, C. B. Schroeder, E. Esarey, C. G. R. Geddes, and W. P. Leemans, in *Proceedings of 2010 AAC Workshop*, edited by G. Nusinovich and S. Gold (AIP, NY, 2010), Vol. 1299, p. 250-255.
- <sup>32</sup>C. Benedetti, C. B. Schroeder, E. Esarey, and W. P. Leemans, in *Proceedings of PAC11 (JACoW, 2011)* p. MOP082.
- <sup>33</sup>C. Benedetti, C. B. Schroeder, E. Esarey, and W. P. Leemans, in *Proceedings of ICAP12 (JACoW, 2012)* p. THAI02.
- <sup>34</sup>W. Lu, C. Huang, M. Zhou, W. B. Mori, and T. Katsouleas, *Phys. Rev. Lett.* **96**, 165002 (2006).
- <sup>35</sup>E. Cormier-Michel, B. A. Shadwick, C. G. R. Geddes, E. Esarey, C. B. Schroeder, and W. P. Leemans, *Phys. Rev. E* **78**, 016406 (2008).
- <sup>36</sup>F. S. Tsung, Ritesh Narang, W. B. Mori, C. Joshi, R. A. Fonseca, and L. O. Silva, *Phys. Rev. Lett.* **93**, 185002 (2004).
- <sup>37</sup>S. Y. Kalmykov, S. A. Yi, A. Beck, A. F. Lifschitz, X. Davoine, E. Lefebvre, A. Pukhov, V. Khudik, G. Shvets, S. A. Reed, P. Dong, X. Wang, D. Du, S. Bedacht, R. Zgadzaj, W. Henderson, A. Bernstein, G. Dyer, M. Martinez, E. Gaul, T. Ditmire, and M. C. Downer, *New J. Phys.* **12**, 045019 (2010).
- <sup>38</sup>C. Benedetti, A. Sgattoni, G. Turchetti, and P. Londrillo, *IEEE Trans. Plasma Sci.* **36**, 1790 (2008).
- <sup>39</sup>C. Benedetti, P. Londrillo, V. Petrillo, L. Serafini, A. Sgattoni, P. Tomassini, G. Turchetti, *Nucl. Instrum. Meth. A* **608**, S94 (2009).
- <sup>40</sup>C. Benedetti, C. B. Schroeder, E. Esarey, and W. P. Leemans, *Phys. Plasmas* **19**, 053101 (2012).
- <sup>41</sup>P. Volfbeyn, E. Esarey, and W. P. Leemans, *Phys. Plasmas* **6**, 2269 (1999).
- <sup>42</sup>M. C. Marconi, C. H. Moreno, J. J. Rocca, V. N. Shlyaptsev, and A. L. Osterheld, *Phys. Rev. E* **62**, 7209 (2000).
- <sup>43</sup>C. B. Schroeder, and E. Esarey, *Phys. Rev. E* **81**, 056403 (2010).